# SUPERVISED CLASSIFICATION OF SCATTERERS ON SAR IMAGING BASED ON INCOHERENT POLARIMETRIC TIME-FREQUENCY SIGNATURES

*M. Duquenoy*[1,2]*, J.P. Ovarlez*[1,3]*, L. Ferro-Famil*[2] *and E. Pottier*[2]

[1] ONERA, The French Aerospace lab / DEMR / Signal processing unit
Chemin de la Hunière, F-91761, Palaiseau cedex, France
phone: + (33).1.69.93.63.13, fax: + (33).1.69.93.62.69.
email: mickael.duquenoy@gmail.com, jean-philippe.ovarlez@onera.fr

[2] IETR, Image and Remote Sensing Group / SAPHIR Team
University of Rennes 1, Campus Beaulieu, Bat 11D, 263 avenue du Général Leclerc
CS-74205 Rennes cedex, France
phone: + (33).2.23.23.67.14, fax: + (33).2.23.23.69.63.
email: laurent.ferro-famil@univ-rennes1.fr, eric.pottier@univ-rennes1.fr

[3] SONDRA, Supelec, Plateau du Moulon, 3 rue Joliot-Curie, F-91192 Gif-sur-Yvette Cedex, France

## ABSTRACT

This paper deals with the analysis of the non-stationary behavior of scatterers in polarimetric SAR imaging . A method based on continuous wavelet and incoherent polarimetric decompositions is proposed to extract the polarimetric time-frequency signatures of scatterers. These signatures characterize scatterers according to their polarimetric /or energetic behavior versus the emitted frequency and the observation angle. Then, signatures from reference targets are used to train a multi-layer perceptron (MLP). All in all, SAR imaging data are classified by the MLP. The efficiency of this method is demonstrated, for the deterministic targets (man-made targets). It can be explained by the fact that the man-made targets present a strong non-stationary behavior. But for the vegetation and canopy the results are not convincing. It can be interpreted by the fact that the behavior of vegetation is stationary.

## 1. INTRODUCTION

This paper suggests a classification based on polarimetric time-frequency signatures for wideband and strong angular excursion SAR imaging. Indeed, in this case the model of bright point is not valid. Time-frequency analysis allows to build HyperImages [1], [2], [3] to correct this main drawback. Polarimetry is another information source to characterize scatterers. The aim of this paper is to use jointly time-frequency analysis and polarimetry incoherent decomposition to extract polarimetric time-frequency signatures and use them in a neural network to classify scatterers.

## 2. CONSTRUCTION OF THE HYPER-SCATTERING MATRIX BASED ON THE CONTINUOUS WAVELET

### 2.1 Classical radar imaging

The model usually used in radar imaging is the model of bright points [4]. The object under analysis can be seen as a set of bright points, i.e. a set of independent sources that reflect in the same way for all frequencies (white points) and all directions of presentation (isotropic points). Let $S(\mathbf{r})$ be the complex amplitude of the bright point response located at $\mathbf{r} = (x,y)^T$ in a set of cartesian axes related to the object. Under far field conditions (decomposition into planes waves), the complex backscattering coefficient for the whole object is then given by the in-phase summation of each reflector contribution:

$$H(\mathbf{k}) = \int S(\mathbf{r})\, e^{-2i\pi \mathbf{k}.\mathbf{r}}\, d\mathbf{r}. \tag{1}$$

After a Fourier Transform of (1), one can obtain the spatial distribution $I(\mathbf{r})$ of the reflectors complex amplitude for a mean frequency (the center frequency) and for a mean angle of presentation:

$$S(\mathbf{r}) = \int H(\mathbf{k})\, e^{2i\pi \mathbf{k}.\mathbf{r}}\, d\mathbf{k}. \tag{2}$$

The spatial distribution of the scatterers energy will be denoted in the following by:

$$\tilde{I}(\mathbf{r}) = |S(\mathbf{r})|^2 \tag{3}$$

A full polarimetric radar is generally designed to transmit and receive microwave radiations horizontally ($h$) or vertically ($v$) polarized. The polarimetric generalization of the scattering coefficient is called the scattering matrix $[\mathbf{S}]$ or Sinclair matrix:

$$[\mathbf{S}(\mathbf{r})] = \begin{bmatrix} S_{hh}(\mathbf{r}) & S_{hv}(\mathbf{r}) \\ S_{vh}(\mathbf{r}) & S_{vv}(\mathbf{r}) \end{bmatrix}. \tag{4}$$

When a target is illuminated by a broad-band signal and/or for a large angular extent, it is realistic to consider that the spatial distribution $\tilde{I}(\mathbf{r})$ of the reflectors energy (or the Sinclair complex image $S(\mathbf{r})$) depends on frequency $f$ and on illumination angle $\theta$. These two amplitude and energy distributions depending on the vector $\mathbf{k}$, they will be denoted respectively by $S(\mathbf{r},\mathbf{k})$ and $\tilde{I}(\mathbf{r},\mathbf{k})$ in the sequel.

### 2.2 Extended radar imaging

Let $\phi(\mathbf{k})$ be a mother wavelet supposed to represent the signal reflected by a reference target. This target is supposed

located around $\mathbf{r} = \vec{0}$ and backscatters the energy in the direction $\theta = 0$ and at the frequency $f$ given by $k = \frac{2f}{c} = 1$. A family of function is built $\Psi_{\mathbf{r}_0,\mathbf{k}_0}$ from $\phi(\mathbf{k})$ by the similarity group $S$ [1], [2]:

$$\Psi_{\mathbf{r}_o,\mathbf{k}_o}(\mathbf{k}) = \frac{1}{k_o}\, e^{-j2\pi\mathbf{k}.\mathbf{r}_o} \phi\left(\frac{1}{k_o}\mathscr{R}_{\theta_o}^{-1}\,\mathbf{k}\right) \quad (5)$$

$$= \frac{1}{k_o}\, e^{-j2\pi\mathbf{k}.\mathbf{r}_o}\, \phi\left(\frac{k}{k_o}, \theta - \theta_o\right). \quad (6)$$

The wavelet coefficient $S_{xx}(\mathbf{r}_o,\mathbf{k}_o)$ is defined as the scalar product between the complex backscattering coefficient $H_{xx}$ and the wavelet $\Psi_{\mathrm{r_o,k_o}}$:

$$S_{xx}(\mathbf{r}_o,\mathbf{k}_o) = < H_{xx}, \Psi_{\mathbf{r}_o,\mathbf{k}_o} > \quad (7)$$

The scalar product is defined following [5]:

$$S_{xx}(\mathbf{r}_o,\mathbf{k}_o) = \int_0^{2\pi} d\theta \int_0^{+\infty} k\, H_{xx}(k,\theta)\, \frac{1}{k_o} e^{+j2\pi\mathbf{k}.\mathbf{r}_o} \phi^*\left(\frac{k}{k_o}, \theta - \theta_o\right) dk \quad (8)$$

The scalogram which is the square modulus of the wavelet coefficients defines the hyperImage $\tilde{I}(\mathbf{r},\mathbf{k})$.

### 2.3 Properties

The continuous wavelet transform has two interesting properties. The first is the reconstruction: it is possible to rebuild the complex backscattering coefficient $H_{xx}(\mathbf{k})$ from the wavelet coefficient $S_{xx}(\mathbf{r}_o,\mathbf{k}_o)$:

$$H_{xx}(\mathbf{k}) = \frac{1}{K_\phi} \int_S d\mathbf{r}_o \int S_{xx}(\mathbf{r}_o,\mathbf{k}_o)\, \Psi_{\mathbf{r}_o,\mathbf{k}_o}(\mathbf{k})\, d\mathbf{k}_o \quad (9)$$

with $K_\phi$ defined as the *admissibility coefficient* of the mother wavelet which must, to build $H_{xx}(\mathbf{k})$ from the wavelet coefficients, check:

$$K_\phi = \int |\phi(\mathbf{k})|^2\, \frac{d\mathbf{k}}{k^2} < +\infty \quad (10)$$

The second property is the isometry:

$$\frac{1}{K_\phi} \int_S d\mathbf{r}_o \int |S_{xx}(\mathbf{r}_o,\mathbf{k}_o)|^2\, d\mathbf{k}_o = \|H_{xx}\|^2 \quad (11)$$

### 2.4 Limitations

The continuous wavelet is limited by the Heisenberg principle. Indeed, this concept tells that we cannot obtain a spatial good resolution with a good resolution in the frequency domain and reciprocally. However, the continuous wavelet offers a resolution which changes with the frequency and the spatial domain. It allows multiresolution analysis [6].

### 2.5 Hyper-Scattering matrix definition and extended Span

The wavelet transform is applied on each of the four polarimetric channels. The resulting Sinclair scattering matrix now depends on the frequency and on the illumination angle and is called hyper-scattering matrix:

$$[\mathbf{S}](\mathbf{r},\mathbf{k}) = \begin{bmatrix} S_{hh}(\mathbf{r},\mathbf{k}) & S_{hv}(\mathbf{r},\mathbf{k}) \\ S_{vh}(\mathbf{r},\mathbf{k}) & S_{vv}(\mathbf{r},\mathbf{k}) \end{bmatrix}. \quad (12)$$

The span is generally defined as the sum of the squared modulus of each element of the matrix (4). The extended span is now defined as the sum of the squared modulus of each element of the hyper-scattering matrix (12).

$$P(\mathbf{r},\mathbf{k}) = |S_{hh}(\mathbf{r},\mathbf{k})|^2 + |S_{hv}(\mathbf{r},\mathbf{k})|^2 + |S_{vh}(\mathbf{r},\mathbf{k})|^2 + |S_{vv}(\mathbf{r},\mathbf{k})|^2. \quad (13)$$

The extended span provides a first polarimetric time-frequency signatures. Indeed, if one scatterer is selected at the position $\mathbf{r}_0$, $P(\mathbf{r}_0,\mathbf{k})$ describes the polarimetric energetic behavior of this scatterer versus the emitted frequency and the observation angle.

## 3. CONSTRUCTION OF THE INCOHERENT POLARIMETRIC TIME-FREQUENCY SIGNATURES

### 3.1 Definition of the covariance and coherency matrix

A scattering vector can be obtained by the projection of the Sinclair matrix on an orthogonal basis of special unitary group [7]. The two bases which are the most used, are the the lexicographic basis and the Pauli basis. In monostatic scenario, the reciprocity theorem holds and hence: $S_{hv} = S_{vh}$. So, by projecting the hyper-scattering matrix on the two bases, two hyper-scattering vectors which contain all polarimetric information can be obtained:

$$k_L(\mathbf{r},\mathbf{k}) = [S_{hh}(\mathbf{r},\mathbf{k}), \sqrt{2}S_{hv}(\mathbf{r},\mathbf{k}), S_{vv}(\mathbf{r},\mathbf{k})]^T \quad (14)$$

$$k_P(\mathbf{r},\mathbf{k}) = \frac{1}{\sqrt{2}}[S_{hh}(\mathbf{r},\mathbf{k}) + S_{vv}(\mathbf{r},\mathbf{k}), S_{hh}(\mathbf{r},\mathbf{k}) - S_{vv}(\mathbf{r},\mathbf{k}), 2S_{hv}(\mathbf{r},\mathbf{k})]^T \quad (15)$$

where $^T$ is the transpose operator.

From these targets vectors, the covariance hyper-matrix $[C(\mathbf{r},\mathbf{k})]$ and the coherency hyper-matrix $[T(\mathbf{r},\mathbf{k})]$ can be defined:

$$[C(\mathbf{r},\mathbf{k})] = \langle k_L(\mathbf{r},\mathbf{k}) k_L^{*T}(\mathbf{r},\mathbf{k}) \rangle \quad (16)$$

$$[T(\mathbf{r},\mathbf{k})] = \langle k_P(\mathbf{r},\mathbf{k}) k_P^{*T}(\mathbf{r},\mathbf{k}) \rangle \quad (17)$$

where $^*$ and $\langle\rangle$ are respectively the conjugate and the statistical mean operators.

The aim of this part is to use incoherent decompositions to obtain polarimetric time-frequency signatures. Hence, The objective of the incoherent decompositions is to separate the covariance or coherency matrices as the combination of second order descriptors corresponding to simpler or canonical objects, presenting an easier physical interpretation [8].

$$[C(\mathbf{r},\mathbf{k})] = \sum_{i=1}^{k} p_i(\mathbf{r},\mathbf{k})[C(\mathbf{r},\mathbf{k})]_i \quad (18)$$

$$[T(\mathbf{r},\mathbf{k})] = \sum_{i=1}^{k} q_i(\mathbf{r},\mathbf{k})[T(\mathbf{r},\mathbf{k})]_i \quad (19)$$

where the canonical responses are represented by $C[(\mathbf{r},\mathbf{k})]_i$ and $T[(\mathbf{r},\mathbf{k})]_i$, and $p_i(\mathbf{r},\mathbf{k})$ and $q_i(\mathbf{r},\mathbf{k})$ denote the coefficients of these components.

### 3.2 The Freeman-Durden Decomposition

*3.2.1 Construction of the polarimetric time-frequency signatures*

By applying the Freeman-Durden decomposition [9] on the covariance hyper-matrix, we obtain the three components scattering mechanism model:

$$\begin{aligned}[C(\mathbf{r},\mathbf{k})] &= f_s(\mathbf{r},\mathbf{k})[C(\mathbf{r},\mathbf{k})]_s + f_d(\mathbf{r},\mathbf{k})[C(\mathbf{r},\mathbf{k})]_d \\ &\quad + f_v(\mathbf{r},\mathbf{k})[C(\mathbf{r},\mathbf{k})]_v \end{aligned} \quad (20)$$

where $f_s(\mathbf{r},\mathbf{k})[C(\mathbf{r},\mathbf{k})]_s$ represents the single scattering, $f_d(\mathbf{r},\mathbf{k})[C(\mathbf{r},\mathbf{k})]_d$ is the double scattering and $f_v(\mathbf{r},\mathbf{k})[C(\mathbf{r},\mathbf{k})]_v$ the volume scattering. To calculate the different parameters, there are four observed equations for five unknown real coefficients:

$$\begin{aligned}[C(\mathbf{r},\mathbf{k})]_{1,1} &= f_s(\mathbf{r},\mathbf{k})\beta(\mathbf{r},\mathbf{k})^2 + f_d(\mathbf{r},\mathbf{k})\alpha(\mathbf{r},\mathbf{k})^2 \\ &\quad + f_v(\mathbf{r},\mathbf{k}) \\ [C(\mathbf{r},\mathbf{k})]_{1,3} &= f_s(\mathbf{r},\mathbf{k})\beta(\mathbf{r},\mathbf{k}) - f_d(\mathbf{r},\mathbf{k})\alpha(\mathbf{r},\mathbf{k}) \\ &\quad + \frac{f_v(\mathbf{r},\mathbf{k})}{3} \\ [C(\mathbf{r},\mathbf{k})]_{2,2} &= \frac{2f_v(\mathbf{r},\mathbf{k})}{3} \\ [[C(\mathbf{r},\mathbf{k})]_{3,1} &= f_s(\mathbf{r},\mathbf{k})\beta(\mathbf{r},\mathbf{k}) - f_d(\mathbf{r},\mathbf{k})\alpha(\mathbf{r},\mathbf{k}) \\ &\quad + \frac{f_v(\mathbf{r},\mathbf{k})}{3} \\ [[C(\mathbf{r},\mathbf{k})]_{3,3} &= f_s(\mathbf{r},\mathbf{k}) + f_d(\mathbf{r},\mathbf{k}) + f_v(\mathbf{r},\mathbf{k}) \end{aligned} \quad (21)$$

So, an assumption is made [9]:

- if $\mathscr{R}e\{\langle S_{hh}(\mathbf{r},\mathbf{k})S(\mathbf{r},\mathbf{k})^*_{vv}\rangle - \frac{f_v(\mathbf{r},\mathbf{k})}{3}\} > 0 \rightarrow \alpha(\mathbf{r},\mathbf{k}) = 1$
- if $\mathscr{R}e\{\langle S_{hh}(\mathbf{r},\mathbf{k})S(\mathbf{r},\mathbf{k})^*_{vv}\rangle - \frac{f_v(\mathbf{r},\mathbf{k})}{3}\} < 0 \rightarrow \beta(\mathbf{r},\mathbf{k}) = 1$

Consequently the different parameters can be processed.

*3.2.2 Interpretation of the polarimetric time-frequency signatures*

The term $f_v(\mathbf{r},\mathbf{k})$ corresponds to the contribution of the volume scattering of the final hyper-covariance matrix. Hence, the scattered power by this component can be written as follows:

$$P_v(\mathbf{r},\mathbf{k}) = \frac{8f_v(\mathbf{r},\mathbf{k})}{3} \quad (22)$$

The power scattered by the double-bounce component of the hyper-covariance matrix has the expression:

$$P_d(\mathbf{r},\mathbf{k}) = f_d(\mathbf{r},\mathbf{k})(1+|\alpha(\mathbf{r},\mathbf{k})|^2) \quad (23)$$

Finally, the power scattered by the surface-like component is:

$$P_s(\mathbf{r},\mathbf{k}) = f_s(\mathbf{r},\mathbf{k})(1+|\beta(\mathbf{r},\mathbf{k})|^2) \quad (24)$$

For a scatterer located at $\mathbf{r_0}$, $P_v(\mathbf{r_0},\mathbf{k})$ (respectively, $P_d(\mathbf{r_0},\mathbf{k})$, and $P_s(\mathbf{r_0},\mathbf{k})$) represents the polarimetric behavior of volume scattering (respectively double scattering and simple scattering) versus the emitted frequency and the observation angle. These representations are called polarimetric time-frequency signatures.

### 3.3 The H/A/Alpha decomposition

*3.3.1 Construction of the polarimetric time-frequency signatures*

An Hermitian matrix $3\times 3$ can be factorized according to [7], [10]:

$$T(\mathbf{r},\mathbf{k}) = P(\mathbf{r},\mathbf{k})D(\mathbf{r},\mathbf{k})P(\mathbf{r},\mathbf{k})^{-1} \quad (25)$$

The matrix $D(\mathbf{r},\mathbf{k})$ is diagonal with three real eigenvalues $\lambda_1(\mathbf{r},\mathbf{k}) > \lambda_2(\mathbf{r},\mathbf{k}) > \lambda_3(\mathbf{r},\mathbf{k})$ The unitary matrix is composed with eigenvectors whose the form is:

$$\begin{aligned}P_k(\mathbf{r},\mathbf{k}) = [&\cos(\alpha_k(\mathbf{r},\mathbf{k})), \sin(\alpha_k(\mathbf{r},\mathbf{k}))\cos(\beta_k(\mathbf{r},\mathbf{k})) \\ &\exp(j\delta_k(\mathbf{r},\mathbf{k})), \sin(\alpha_k(\mathbf{r},\mathbf{k}))\cos(\beta_k(\mathbf{r},\mathbf{k}))\exp(j\gamma_k(\mathbf{r},\mathbf{k}))]^T\end{aligned}$$

So, the decomposition can be written according to:

$$[T(\mathbf{r},\mathbf{k})] = \sum_{k=1}^{3} \lambda_k(\mathbf{r},\mathbf{k})P_k(\mathbf{r},\mathbf{k})P_k(\mathbf{r},\mathbf{k})^{*T} \quad (26)$$

From these eigenvectors and eigenvalues, secondary characteristics parameters can be extracted. Indeed, the eigenvalues show the power of each mechanism of the decomposition. The eigenvalues can be normalized following [8]:

$$p_k(\mathbf{r},\mathbf{k}) = \frac{\lambda_k(\mathbf{r},\mathbf{k})}{\sum_{k=1}^{3}\lambda_k(\mathbf{r},\mathbf{k})} \quad (27)$$

So, the entropy can be processed to determine the degree of randomness of the scattering process, which can be also interpreted as the degree of statistical disorder:

$$H(\mathbf{r},\mathbf{k}) = -\sum_{k=1}^{3} p_k(\mathbf{r},\mathbf{k})\log_3(p_k(\mathbf{r},\mathbf{k})) \quad (28)$$

The anisotropy can be defined to describe the secondary mechanisms:

$$A(\mathbf{r},\mathbf{k}) = \frac{p_2(\mathbf{r},\mathbf{k}) - p_3(\mathbf{r},\mathbf{k})}{p_2(\mathbf{r},\mathbf{k}) + p_3(\mathbf{r},\mathbf{k})} \quad (29)$$

The last parameter of the decomposition indicates the nature of the mechanism:

$$\alpha(\mathbf{r},\mathbf{k}) = \sum_{k=1}^{3} p_k(\mathbf{r},\mathbf{k})\alpha_k(\mathbf{r},\mathbf{k}) \quad (30)$$

*3.3.2 Interpretation of the polarimetric time-frequency signatures*

For a scatterer located at $\mathbf{r_0}$, $H(\mathbf{r_0},\mathbf{k})$ (respectively, $A(\mathbf{r_0},\mathbf{k})$, and $\alpha(\mathbf{r_0},\mathbf{k})$) represents the entropy (anisotropy and the $\alpha$ parameter) versus the emitted frequency and the observation angle. These representations are called polarimetric time-frequency signatures.

## 4. SUPERVISED CLASSIFICATION USING NEURAL NETWORKS

Neural networks are non-linear statistical data modeling tools. They can be used to find pattern data [11].

### 4.1 Architecture of the multi-layer perceptron (MLP)

A multi-layer perceptron is a feedforward artificial neural network model that maps sets of input data onto a set of appropriate output. The structure of our multi-layer perceptron is described figure (1). It is composed of nodes whose the processing is [12]:

$$a_j^{(1)} = \sum_{i=1}^{d} w_{ij}^{(1)} x_i + b_j^{(1)}, \tag{31}$$

where $a_j^{(1)}$ associated input with each hidden unit. Here $w_{ij}^{(1)}$ represents the elements of the first-layer weight matrix and $b_j$ are the bias parameters associated with the hidden unit.

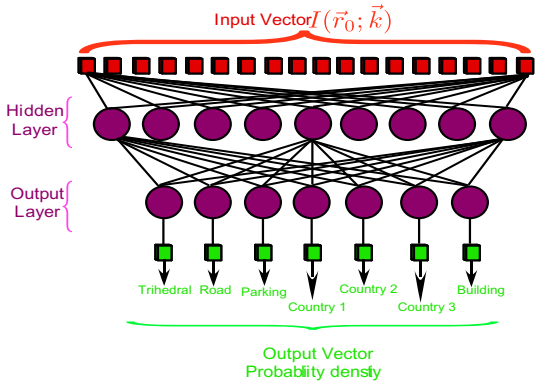


Figure 1: Architecture of the multi-layer perceptron

The variables $a_j^{(1)}$ are then transformed by the non-linear activation function of the hidden layer. The activation function is $\tanh(.)$. The outputs of the hidden units are given by:

$$z_j = \tanh(a_j^{(1)}) \tag{32}$$

which has the property that:

$$\frac{dz_j}{da_j^{(1)}} = 1 - z_j^2 \tag{33}$$

The $z_j$ are then transformed by the second layer of weights and biases to give second-layer activation values $a_k^{(2)}$:

$$a_k^{(2)} = \sum_{j=1}^{M} w_{ij}^{(2)} z_j + b_k^{(2)} \tag{34}$$

Finally, these values are passed through the output-unit activation function to give output values $y_k$. For the more usual kind of classification problem in which we have of c mutually exclusive classes, we use the softmax activation function of the form [12]:

$$y_k = \frac{\exp(a_k^{(2)})}{\sum_{k'} a_{k'}^{(2)}} \tag{35}$$

Our multi-layer perceptron is a three layers whose the number of nodes of the input layer is equal to the number of input, the output layer is equal to the number of class to obtain a probability density whose the maximum defines the class which the scatterer is and the number of nodes of the hidden-layer is calculated following:

$$N_{Hidden-Layer} = \sqrt{N_{input} N_{output}} \tag{36}$$

### 4.2 Learning Basis

In supervised learning, a set of known signatures is given and the aim is to find a function in the allowed class of functions that matches the examples. The cost function is related to the mismatch between the mapping and the data and it implicitly contains prior knowledge about the pattern recognition problem.

The choice of the mother wavelet is moving toward a Gaussian shape. Indeed, a Gaussian have good properties and it has proved itself [13]. The spreading band of the Gaussian is chosen to $\frac{1}{6}$ band because it represents the best compromise of resolution between spatial and frequency domains. Indeed, we want a good resolution on frequency domain.

The polarimetric time-frequency signatures of manually selected scatterers are extracted as explained in the former part. On the image, the scatterers selected are the trihedral, the parking, the building, the road and three countries.

An example of Freeman-Durden learning basis is presented on the figure 2. The three contributions are coded respectively: $P_d$ in red, $P_v$ in green and $P_s$ in blue. The image in the center is the image full resolution of the Freeman-Durden decomposition.

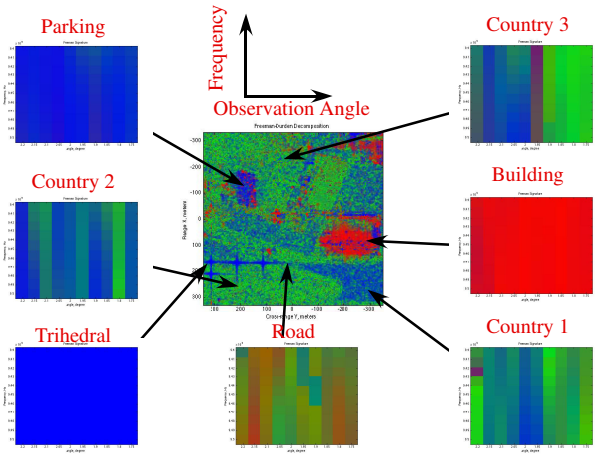


Figure 2: Learning basis obtained by the Freeman Durden polarimetric time-frequency signatures

## 5. RESULTS

The data under study is the full resolution image, (see Fig. 2). It is a X band image with an angular excursion of two degrees. The polarimetric time-frequency signatures are processed as explained in the former part. Then, these signatures are sent to the neural networks.

### 5.1 Freeman-Durden polarimetric time-frequency signatures

The results of the Freeman-Durden time-frequency signatures are represented on the figure 3. The trihedrals are classified as trihedral. The parking is identified by a melting pot of parking and trihedral contributions. It can be explained by their signatures. The three buildings are identified as a building. For the vegetation the results show that time-frequency analysis is not sufficient for these behaviors.

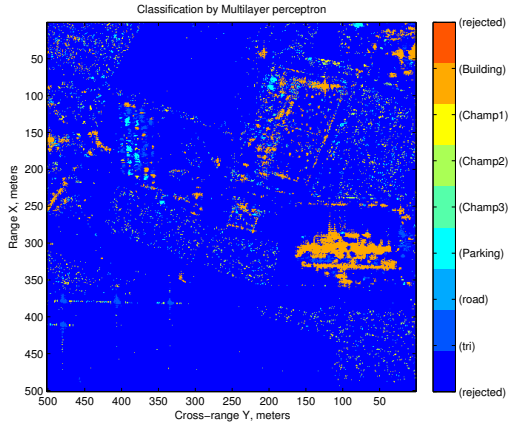


Figure 3: Classification results obtained by the Freeman Durden polarimetric time-frequency signatures

### 5.2 H/alpha polarimetric time-frequency signatures

The results of the H/Alpha time-frequency signatures are described on the figure 4. The trihedrals are classified as trihedral. The parking is identified by a melting pot of parking and trihedral contributions. It can be explained by their signatures. The three buildings are identified as a building. For the vegetation the results show that time-frequency analysis is not sufficient for these behaviors.

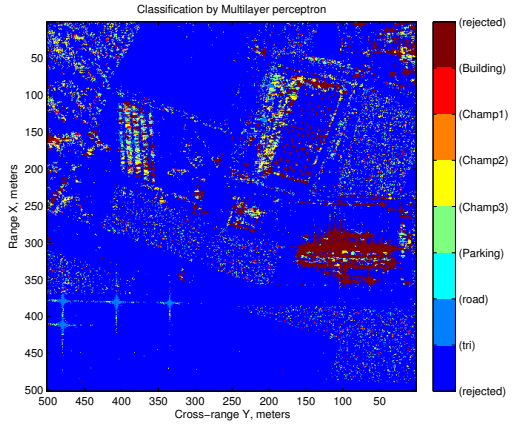


Figure 4: Classification results obtained by the H/A/Alpha polarimetric time-frequency signatures

## 6. CONCLUSION

A new method to classify scatterers on SAR imaging is proposed. This method is designed to work in wideband and strong angular excursion: Very High Resolution image (VHR). Indeed, it is based on stationary or non-stationary behavior of scatterers during the SAR integration. So, time-frequency analysis and polarimetric incoherent decompositions highlight this point of view. The results show that the information from polarimetric time-frequency signatures is valuable for deterministic targets (man-made targets) like trihedral, building and parking. However, this information does not allow to characterize the vegetation or the canopy.

## REFERENCES


[1] J. Bertrand and P. Bertrand, "The concept of hyperimage in wide-band radar imaging," *IEEE Trans. Geosci. Remote Sensing*, vol. 34, no. 5, pp. 1144–1150, Sep. 1996.

[2] J. P. Ovarlez, L. Vignaud, J. C. Castelli, M. Tria, and M. Benidir, "Analysis of sar images by multidimensional wavelet transform," *IEE Proc. Radar. Sonar. Navig.*, vol. 150, no. 4, pp. 234–241, Aug. 2003.

[3] M. Tria, J. P. Ovarlez, L. Vignaud, J. Castelli, and M. Benidir, "Sar imaging using multidimensional continuous wavelet transform," in *Proc. EURASIP XII European Signal Processing Conference (EUSIPCO'04)*, Wien, Austria, Sep. 6–10, 2004, pp. 1179–1182.

[4] D. Mensa, *High Resolution Radar Imaging*. USA: Artech House, 1981.

[5] M. Tria, "Imagerie radar synthése d'ouverture par analyse en ondelettes continues multidimensionnelles," Ph.D. dissertation, Univ. of Paris-Sud, Paris, France, Nov. 2005.

[6] V. C. Chen and H. Ling, *Time-Frequency Transforms for Radar Imaging and Signal Analysis*. Boston: Artech House, 2002.

[7] S. R. Cloude and E. Pottier, "A review of target decomposition theorems in radar polarimetry," *IEEE Trans. Geosci. Remote Sensing*, vol. 34, no. 2, pp. 498–518, Mar. 1996.

[8] C. Lopez-Martinez, L. Ferro-Famil, and E. Pottier, "Polarimetric decompositions," Institut d'Electronique et de Télécommunication de RENNES (IETR), Tutorial, Jan. 2005.

[9] A. Freeman and S. Durden, "A three component scattering model for polarimetric sar data," *IEEE Trans. Geosci. Remote Sensing*, vol. 36, no. 3, May 1998.

[10] S. R. Cloude and E. Pottier, "An entropy based classification scheme for land applications of polarimetric sar," *IEEE Trans. Geosci. Remote Sensing*, vol. 35, no. 1, pp. 68–78, Jan. 1997.

[11] B. Ripley, *Pattern Recognition and neural networks*. Oxford, 1995.

[12] I. Nabney, *Netlab : Algorithms for pattern recognition*. Springer, 2002.

[13] L. Vignaud, "Wavelet-relax feature extraction in radar images," *IEE Proc. Radar. Sonar. Navig.*, vol. 150, no. 4, pp. 242–246, Aug. 2003.